Journal of Molecular Structure 1254 (2022) 132299

Contents lists available at ScienceDirect

Journal of Molecular Structure

journal homepage: www.elsevier.com/locate/molstr

New Schiff bases with a 2,6-bis(2-aminophenylthio)pyridine moiety acting as glutathione reductase activator and inhibitors: Synthesis and molecular docking studies

Turgay Tunc[a], Ahmet Bugra Ortaakarsu[b], Seda Muhsir Hatipoglu[c], Uğur Kazancı[d], Serdar Karabocek[c], Nevin Karabocek[c], Necmi Dege[d], Nurcan Karacan[b,*]

[a] Department of Chemistry and Process Engineering, Kırşehir Ahi Evran University, Faculty of Engineering and Architecture, Kirsehir, Turkey
[b] Chemistry Department, Gazi University, Science Faculty, Ankara, Turkey
[c] Chemical Technologies Department, Amasya University Technical Vocational School, Amasya, Turkey
[d] Department of Physics, Ondokuz Mayıs University, Faculty of Arts and Sciences, Samsun, Turkey

ARTICLE INFO

Article history:
Received 4 November 2021
Revised 18 December 2021
Accepted 27 December 2021
Available online 4 January 2022

Keywords:
Schiff bases
Glutathione reductase inhibitor
Glutathione reductase activator
Molecular docking

ABSTRACT

2,6-bis(2-aminophenylthio)pyridine was synthesized and identified by x-ray diffraction method. Its new Schiff bases (H_2L^1, H_2L^2, L^3 and L^4) were synthesized and characterized by elemental analysis, FT-IR, LC-MS, ^{1}H NMR and ^{13}C NMR techniques. *in vitro* glutathione reductase activities of the compounds were tested on yeast and human glutathione reductase. L^4 enhanced both glutathione reductase activities, resulting in AC_{50} values of 15.06 μM and 15.89 μM, respectively. H_2L^1, H_2L^2 and L^3 were found to be the inhibitors in the range of 50.09 – 55.23 μM for yeast glutathione reductase, and in the range of 56.12–66.87 μM for human glutathione reductase. According to molecular docking analysis at the xanthine binding site in human glutathione reductase (PDB: 1XAN), 2,6-bis(2-aminophenylthio)pyridine is predicted to have antimalarial property due to having a higher XP docking score than the malaria drug Chloroquine. Also, five binding pockets at the human glutathione reductase (PDB:1GRA) were identified using Sitemap analysis for Schiff bases which are non-competitive inhibitors. IFD-Docking scores were found to correlate with experimental IC_{50} value of H_2L^1, H_2L^2 and L^3. Based on the fact that Schiff bases have higher IFD docking scores at binding pocket-1 than at the active site, it can be predicted that Schiff bases prefer to bind to binding pocket-1 in the presence of natural substrate. The difference in glutathione reductase activities of Schiff bases was attributed to the fact that the conformation of the activator L^4-human GR complex was different from that of other inhibitor Schiff bases-human glutathione reductase complexes. ADMET calculations predicted that synthesized ligands obey the Lipinski Rule (rule of five) and Jorgensen Rule (rule of three).

1. Introduction

Reactive oxygen species (ROS) involved in cellular signaling or physiological processes at low concentrations have a harmful effect when the concentration is too high due to the destruction of cell structure, lipid, DNA, and protein, ultimately leading to cell death. Excessive ROS level can induce oxidative stress by causing imbalance between the production of oxidants and the antioxidant defense systems [1,2]. Oxidative stress is responsible for various pathophysiological diseases like inflammatory bowel diseases, gastro-duodenal ulcers, and malignancies [3]. Recent studies extended this list to metabolic disorders, infectious, neurodegenerative, immune degenerative diseases and others such as asthma, myocardial infarction, colorectal cancer, AIDS as well [2,4].

GSH (L-glutamyl-L-cysteine-L-glycine) is the most abundant low molecular mass thiol, and plays an essential role in protecting cells from oxidative stress. The glutathione system involving glutathione reductases is a major protection system for detoxification of ROS within the red cells [5]. Glutathione reductase (GR) catalyzes the reduction of glutathione disulfide (GSSG) to glutathione (GSH), which increases the GSH/GSSG ratio. Maintaining a high GSH/ GSSG ratio helps balance overall cellular redox potential and diminishes oxidative stress [6]. Hence, GR activator might provide strong protective effects against oxidative stress-related diseases, however, research on GR agonists is scarce [7]. Interestingly, glutathione reductase inhibitors that increase ROS levels and cause oxidative damage were reported to exhibit antimalarial and anticancer activity [8].

* Corresponding author.
E-mail address: nkaracan@gazi.edu.tr (N. Karacan).

https://doi.org/10.1016/j.molstruc.2021.132299
0022-2860/

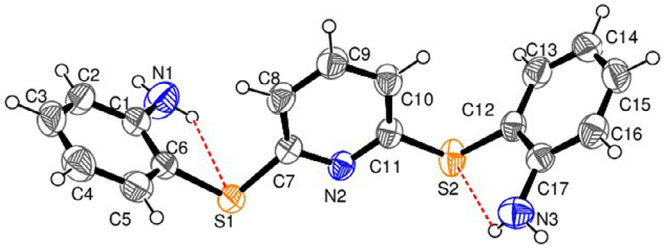

Fig. 1. An ORTEP diagram of the 2,2′-(pyridine-2,6-diyldisulfanediyl)dianiline, with the atom-numbering scheme. Displacement ellipsoids are drawn at the 40% probability level. The intramolecular hydrogen bond is shown as a dashed line.

Schiff bases present different biological activities, including antiviral, antimalarial, antifungal, antibacterial, anticancer, anti-inflammatory, analgesic, antioxidant [9–11] and free radical scavenging properties [12]. Login et.al reported that a novel thiazolyl Schiff base may be used as an adjuvant therapy in diseases caused by excessive free radical production [13]. Balaydın et.al. showed the GR inhibitory activity of a series of Schiff bases bearing triazole ring [14].

Inspired of these finding, toward the discovery of novel GR inhibitors, we synthesized 2,6-bis(2-aminophenylthio)pyridine and its four Schiff bases, and screened their *in vitro* GR activities against yeast GR and human GR. In addition, molecular docking simulation was performed using the X-ray crystallographic structure of the human GR (PDB: 1GRA). Through this study, binding affinity of the compounds in different binding pockets generated by the SiteMap analysis were investigated.

2. Result and discussion

2.1. Crystal structure of 2,2′-(pyridine-2,6-diyldisulfanediyl)dianiline

The crystal structure of the 2,2′-(pyridine-2,6-diyldisulfanediyl)dianiline ($C_{17}H_{15}N_3S_2$) was determined at 296 K. The unit cell parameters of the compound are a = 10.2026 (4) Å, b = 7.3030 (4) Å, c = 21.8564 (12) Å, β = 94.230 (4)°. Centrosymmetric compound crystallizes in the *monoclinic*, space group P21/n with four molecules in the unit cell. An ORTEP drawing with 40% probability displacement ellipsoids and atom-numbering schemes of the compound are shown in Fig. 1. The crystal and instrumental parameters used in the unit-cell determination and data collection are summarized in Table S1. Some selected geometric parameters (bond lengths, bond angles and dihedral angles) of the compound are listed in Table S2.

It contains two phenyl rings (ring A: C1/C2/C3/C4/C5/C6) and (ring B: C12/C13/C14/C15/C16/C17) one pyridine ring (ring C: C7/C8/C9/C10/C11/N2). The three rings are essentially planar but the rings are not coplanar. The maximum deviation of the pyridine ring and the phenyl rings from planarity are 0.0057 Å for atom C11 and −0.0029 Å for atom C5 and 0.0027 Å for atom C12 at C and A and B rings, respectively. The plane of the pyridine ring makes dihedral angles of 85.676 (0.056) and 85.349 (0.056)° with the planes of rings A and B, respectively. Two phenyl rings between dihedral angles is 73.637 (0.046)°. The r.m.s. deviation of the molecule's phenyl rings are 0.0018 Å, 0.0017 Å for A and B rings, respectively and 0.0044 Å for pyridine ring. The aromatic C–C distances for the title compound range from 1.365 (3) Å to 1.399 (2) Å. The crystal structure of the compound has weak intramolecular N–H···S and intermolecular N–H···N hydrogen bonds (Table S3). All the bond distances of the compound are consistent with those of similar compounds [15–17].

2.2. Chemistry

Synthesis of 2,2′-(pyridine-2,6-diyldisulfanediyl)dianiline (P) was accomplished by reaction of 2,6-dichloropyridine and 2-aminobenzenethiol in ethanol-water (1:2) solution. Its derivatives were synthesized by condensation of P with aromatic aldehydes (salicylaldehyde/thiophenecarbaldehyde/1H-imidazole-4-carbaldehyde) and diacethylmonoxime. Their structure was confirmed by ^{1}H NMR, ^{13}C NMR, IR and LC-MS methods. Structures of the compounds were given in Fig. 2.^{1}H NMR chemical shift values of the compounds were given in Table S4.

A strong singlet peak (D_2O exchangeable) at 4.3 ppm in the ^{1}H NMR spectrum of P (given in Supplementary Materials Fig. S1) belongs to amine protons, and disappears with Schiff base and oxime formation. Characteristic peak of the alpha-hydrogen of CH=N as a singlet observed in ^{1}H NMR spectra is a strong indicator of formation of Schiff bases [11]. The imine protons (HC=N) were seen as singlets at 8.60 ppm for H_2L^1 (Fig. S2) 9.80 ppm for L^3 (Fig. S3) and 8.55 ppm for L^4 (Fig. S4). A singlet peak at 9.94 ppm of ^{1}H NMR spectrum of L^4 was attributed to NH protons of imidazole ring. The signal of the phenolic (OH) proton of the H_2L^1 was observed at 12.55 ppm as a singlet peak and disappeared with deuterium exchange. Methyl protons of dioxime (H_2L^2) were seen as singlets at 2.49 ppm (Fig. S5). Hydroxyl proton chemical shift values of oximes are generally reported to range from 8.6 to 13.3 ppm [18], however, we have not observed the oxime proton peaks of H_2L^2, as seen in the other study [19].

The aromatic carbon peaks of P in the ^{13}C NMR spectrum were recorded between 114 – 155 ppm (Fig. S6). However, more carbon peaks in the range of 115 - 182 ppm were observed in the ^{13}C NMR spectra of its derivatives (Figs. S7–S10). Imine carbon peaks were observed at 176.8 ppm (H_2L^1), 181.4 ppm (H_2L^2), 182.1 ppm (L^3), 182.5 ppm (L^4). Two methyl carbon peaks of H_2L^2 were found at 39.3 and 40.5 ppm (Fig. S8).

The mass spectrum of the compounds (Figs. S11–S15) exhibited molecular ion peaks at *m/z* 326.25, 532.74, 512.46 and 479.26, and correspond to $[M+H]^+$ for P, $[M-H]^+$for H_2L^1, $[M-H]^+$ for L^3 and $[M-2H]^+$ for L^4. Molecular ion peak as $[M+5H]^+$ at *m/z* 497.20 for the H_2L^2 is observed. In addition, two fragmentation peaks at *m/z*470.23 and 457.61, corresponding to $[M-OH-4H]^+$ and $[M-2OH-5H]^+$ due to homolytic cleavage of OH bonds were also observed.

In the IR spectrum of the P (Fig. S16), asymmetric and symmetric stretching frequencies of NH_2 were determined at 3374 cm^{-1} and 3295 cm^{-1}, and disappeared with derivative formation. Broad band between 3200 cm^{-1} and 3000 cm^{-1} was assigned to ν(O–) vibration for the H_2L^1 and H_2L^2. ν(C=N) stretching vibrations were observed as sharp bands between 1600 cm^{-1} and 1620 cm^{-1} in all derivatives. The medium band at 3145 cm^{-1} was assigned to ν(N–H) vibration of imidazole ring of L^4.

2.3. Glutathione reductase activity

In order to determine the effects of our compounds on yeast GR and human GR, several concentrations of (5–60 μM) compounds were added into the reaction medium. The enzyme activity was measured and measurements without the use of inhibitors were used as control values (100% activity). IC_{50} values were obtained from activity (%)– concentration plots.% Activity - concentration graph of the H_2L^1 and L^4 for Baker's yeast GR was given in Fig. 3. Total IC_{50} values of the compounds were given in Fig. 4.

As shown, H_2L^1 behaved as the strongest inhibitor against yeast GR (IC_{50} =33.09 μM) and human GR (IC_{50} = 41.12 μM). H_2L^2 is the second most powerful inhibitor against yeast GR (IC_{50} = 42.42 μM) and human GR (IC_{50} = 53.56 μM). Our compounds bearing two hydroxyl groups exhibited improved inhibitory activity. L^3 is the

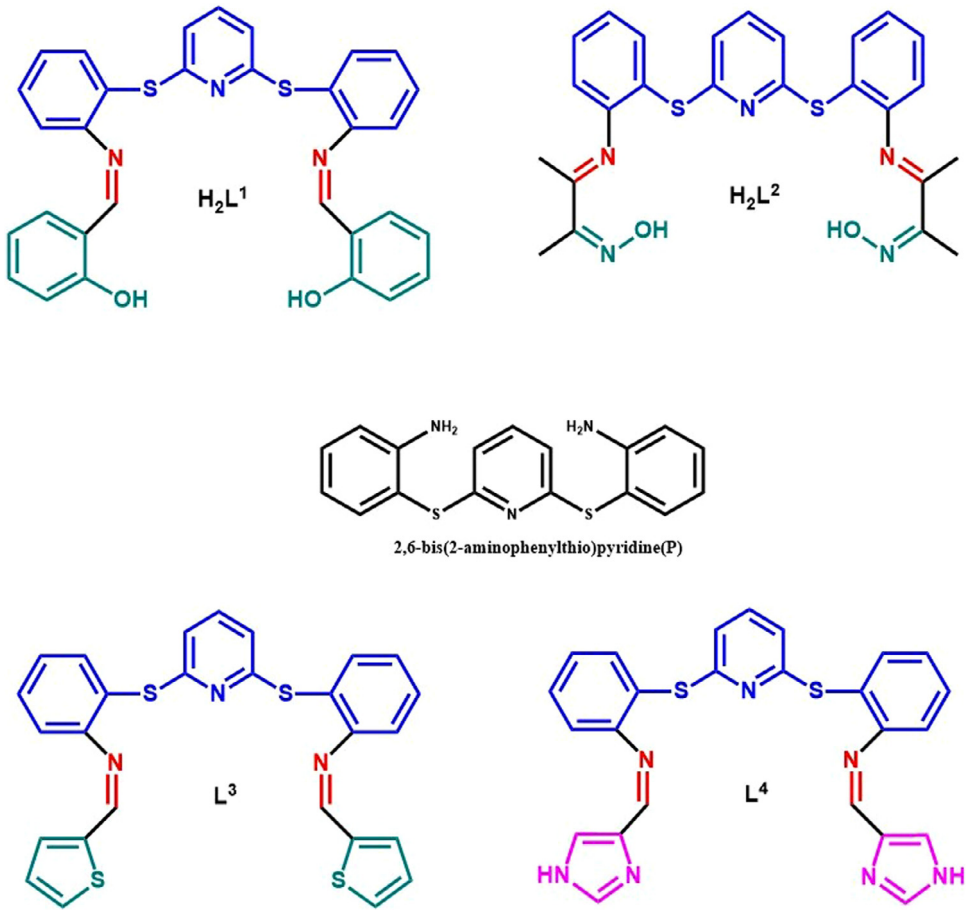

Fig. 2. Structure of the compounds.

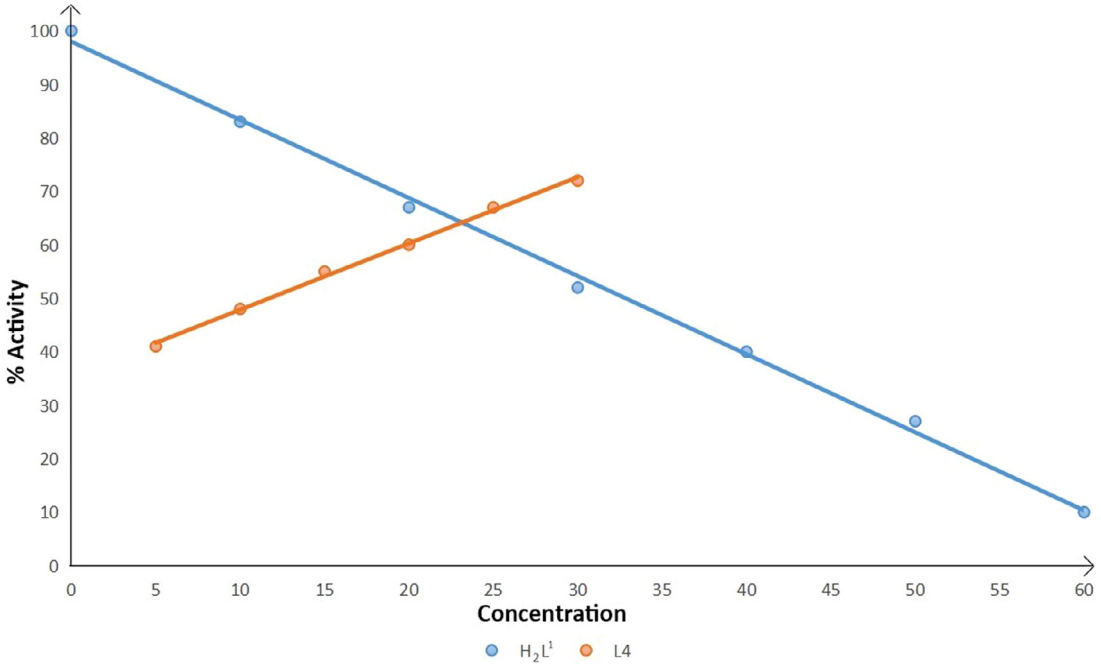

Fig. 3. % Activity - concentration (μM) graph of the H_2L^1 and L^4 for yeast GR.

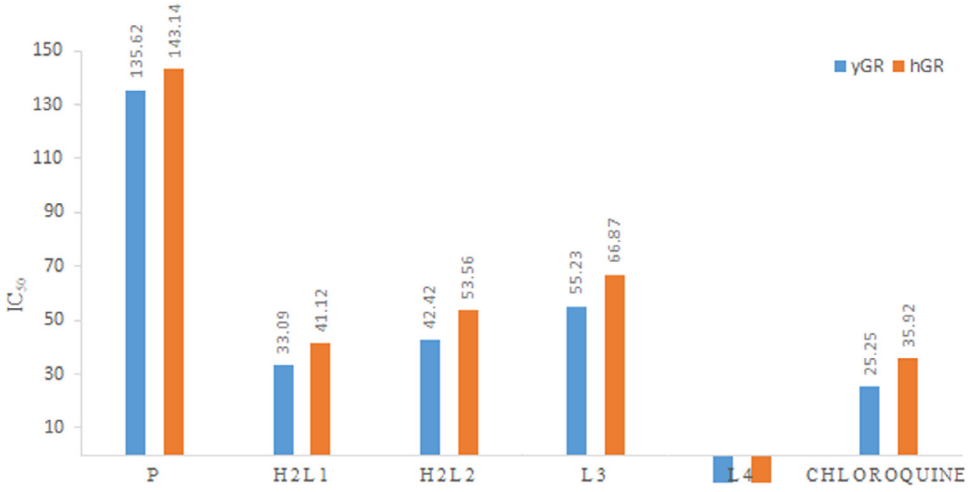

Fig. 4. Bar graph of IC_{50} (μM) values of the compounds for GRs.

third effective inhibitor (IC_{50}values of 55.23 μM and 66.87 μM, respectively). P exhibited the weakest inhibition with IC_{50} values of 135.62 μM and 143.14 μM, respectively. Schiff base bearing thiophene moiety exhibit more inhibitory activity than parent amine. Surprisingly, L^4 acted as an excellent activator against yeast GR (AC_{50} = 12.06 μM) and human GR (AC_{50} = 12.89 μM). Until now, several Schiff bases have been reported as effective GR inhibitors [8,14], however, L^4 is the first Schiff base acting as GR activator. In the author's knowledge, only two potential GR activators, natural Ginsenoside Rb1 [7] and magnesium (2+) cation [20], have been reported in literature. Nitroaromatics are known to be good human GR inhibitors [21]; H_2L^1 shows better human GR inhibitory activity than nitrobenzene (IC_{50}: 546.8 μM) [22], quercetin (57.8 μM) and resveratrol (520 μM) [23].

Human GR and malaria parasite *P.falciparum* GR were identified as targets of antimalarial drugs [24]. Chloroquine (CQ) has been widely used as an antimalarial and autoimmune drug, and also recently in treating COVID-19 [25]. Several pyrazole Schiff bases were found to exhibit *in vitro* antimalarial activity close to that of Chloroquine [26]. In this study, *in vitro* IC_{50} values of Chloroquine were found as 25.25 μM for yeast GR and 35.92 μM for human GR, indicating that our compounds show less inhibitory activity than Chloroquine for both GR. As reported, menadione derivatives behave as the potent inhibitors of both human and *P. falciparum* GR [27]. Non-competitive inhibitor pyocyanin was found to be active against malaria parasite *P. falciparum,* and is directly sandwiched by residues Val74, Phe78, and their symmetry mates Phe78′ and Val74′ of human GR (ID:3SQP). Binding pocket is formed by seven amino acids (Asn71, Val74, His75, Phe78, Tyr407) of one subunit [28]. 10-Arylisoalloxazines which are known to be antimalarial agents, were also found to be sandwiched between the Phe78 residues of the two subunits of human GR [29]. Xanthene also inhibits human GR (PDB:1XAN) in a non-competitive fashion, and binds to the same site mentioned above [30]. So, molecular docking studies were performed for our ligands at the same site in human GR (PDB: 1XAN) using Glide module and XP method (Fig. 5).

Xantane exhibits the best docking score of −7.475, having hydrogen bonding and cation-pi interaction with His82 and Try85. Among our ligands, 2,2′-(pyridine-2,6-diyldisulfanediyl)dianiline (P) showed the second best docking score (−4.376), forming salt bridge with Try407 and Asn71. Pyocyanin and Chloroquine exhibited docking scores of −3.991 and −2.939, showing hydrogen bonding with His82 and salt bridge with Try85, respectively. It can be predicted that P, which has a higher docking score than pyocyanin and chloroquine, may have an antimalarial property. Moreover, homology modeling analysis was carried out using Prime module embedded in the Schrodinger suite. Sequence identity and similarity between human GR (PDB:1GRA) and P. falciparum GR (PDB:1NOF) were found to be 42% and 60% (Fig. 6) indicating that human GR, and *P. falciparum* GR have a high degree of sequence homology. These findings support that P may also have effects on *P. falciparum*.

Fluoro-M5 (menadione derivative) is covalently linked to Cys58 of the active site (GSSG) of the human GR(PDB:2GH5) via a sulfur-carbon bond, but it interacts with the enzyme by additional non-covalent interactions. One keto group of the naphthoquinone is bound via a hydrogen bridge to His467′ of the other subunit. The carboxylate group of the inhibitor side chain is in ionic contact with the active site residues Arg37 and Arg347 and is hydrogen-bonded to Tyr114. Arg37 [27]. Ajoene, a garlic-derived natural compound, is also a covalent inhibitor. The sulfur atom of the ajoene moiety forms the disulfide bridge with Cys58 of human GR (PDB:1BWC). Another direct contact with the protein is to the main chain NH group ofAla34 which is in 3.5-Å distance from the sulfoxo group of the ajoene fragment [31]. On the other hand, some inhibitors have been reported to interact with GR similar to oxidized glutathione (GSSG) by non-covalent bonding such as hydrogen bonds with Ala-34 and Glu-472, π-σ (pi-sigma) dispersion interactions between aliphatic C–H donor groups and aromatic π-acceptors, which are most widely observed in proteins and in peptides [23,32,33].

In this study, we carried out the molecular docking analysis to simulate interactions between our compounds and the active site of human GR(PDB:1GRA). IFD Docking scores (kcal/mol) of the compounds in the active site of human GR is presented in Table 1.

In general, Schiff bases showed higher binding affinity at the larger active site of human GR (PDB:1GRA) than P and Chloroquine, owing to their bulkier structures that afforded more non-covalent interaction. This can be seen when comparing the docking score of P (−5.101 kcal /mol) and H_2L^1(−7.529 kcal/mol), which is also correlated with the experimental IC_{50} values. The binding mode of the Schiff bases into the active site (GSSG) was shown in Fig. 7. The Schiff bases were surrounded by the basic active site residues (Cys58, Cys63, Val58, Lys 66, Try 106, Leu110, Try 114, Ile 343, Thr339, Arg 347, Gln 445).

On the other hand, experimental results show that the Schiff bases act as noncompetitive inhibitors, which can attach at another site of an enzyme, or inhibitor and substrate can both be bound at

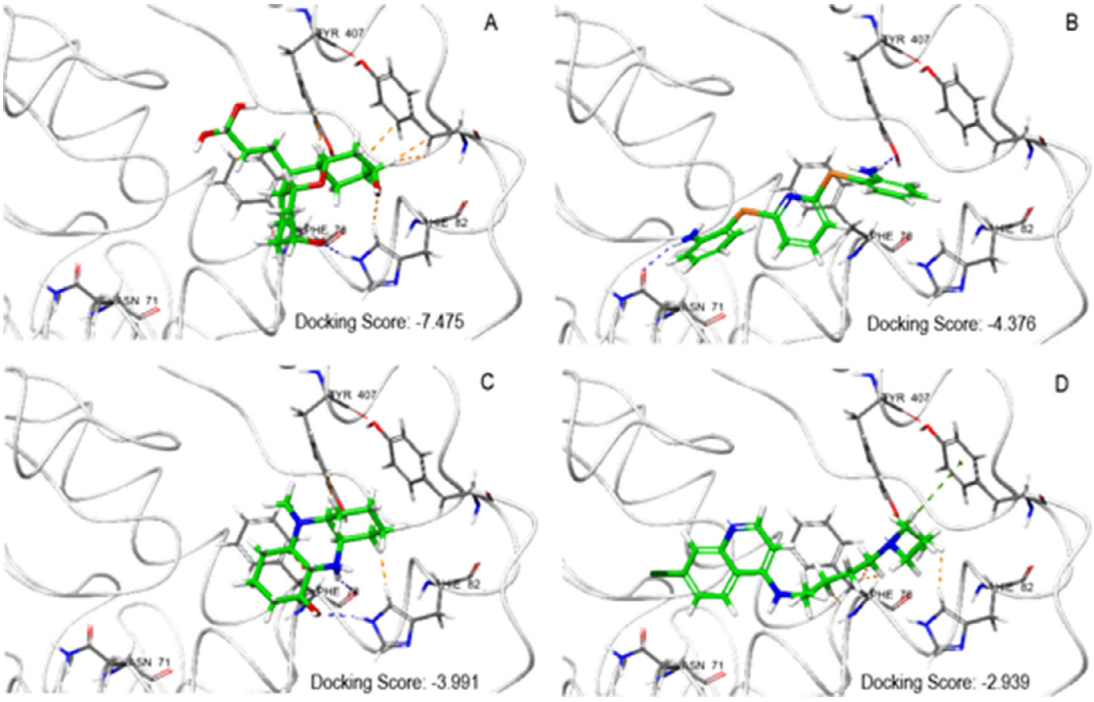

Fig. 5. Human GR (ID:1XAN) structural cartoon models of the ligands with docking score, (A) xantane, (B) 2,2′-(pyridine-2,6-diyldisulfanediyl)dianiline (C) pyocyanin (D) chloroquine.

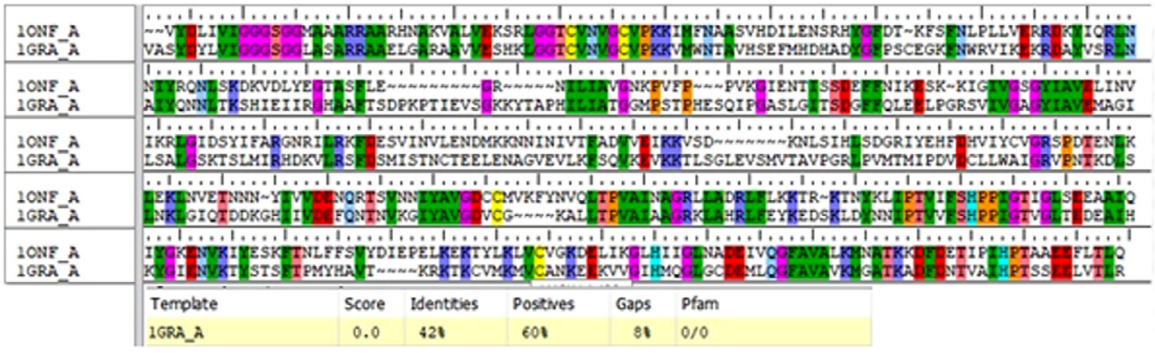

Fig. 6. Amino acid sequence alignment between *P. falciparum* GR (1NOF) and template sequence of human GR (1GRA).

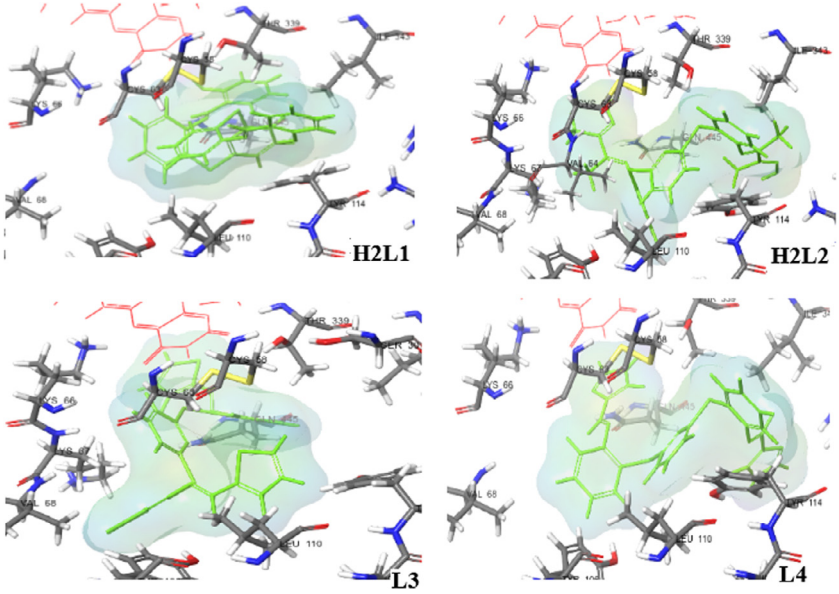

Fig. 7. Molecular docking of the Schiff bases at the active site of GR (PDB:1GRA), Solid surface spans the volume of the Schiff base. FAD (red), Schiff base (green).

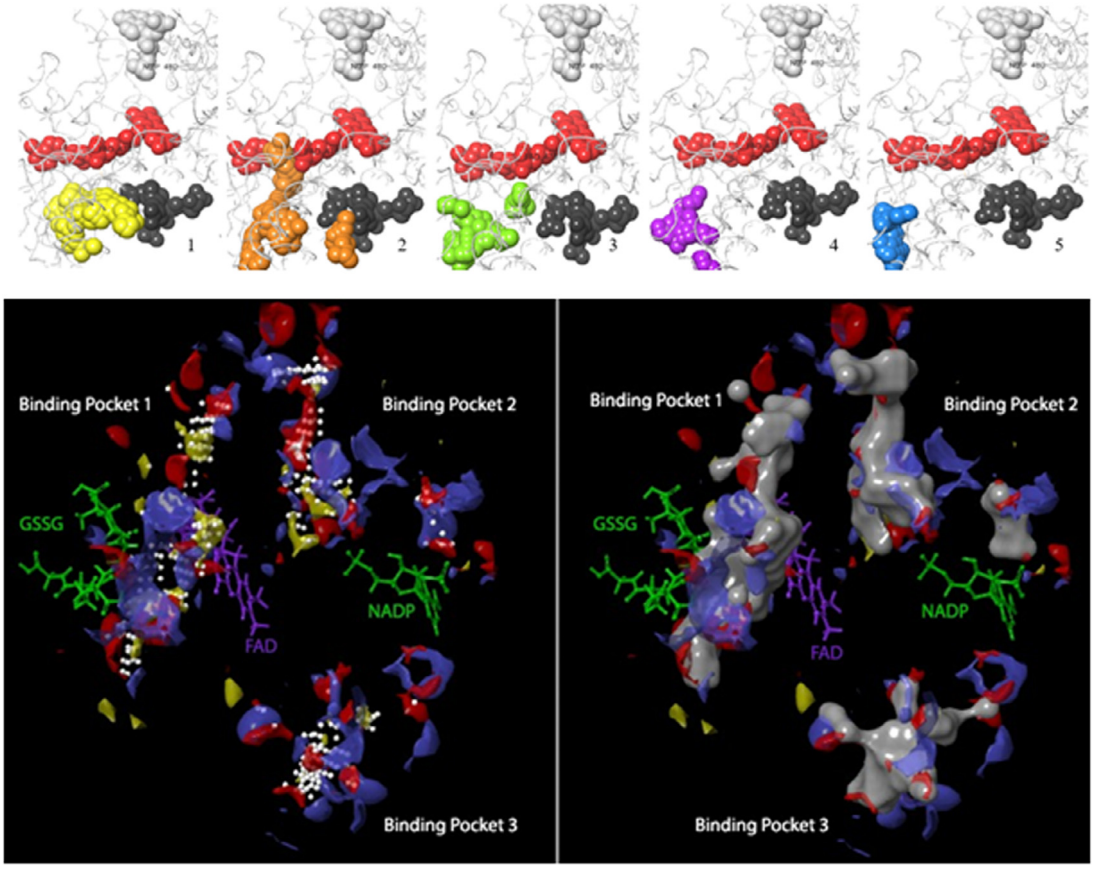

Fig. 8. Binding pockets of the human GR, top: five binding site (yellow, orange, green, violet, blue), FAD(red), GSSG (black), NADP (white); bottom: first three binding pocket with site points (left), and site surface (right) with hydrophobic (yellow), donor (blue) and acceptor (red) domain.

the same time. Therefore, SiteMap module [34] was used to find several other binding sites at which noncompetitive inhibitors may bind (Fig. 8).

SiteScore/size values of five binding pockets (BP) are as follows: 1.068/150 (BP1), 0.998/115 (BP2), 0.866/74 (BP3), 0.732/46 (BP4) and 0.669/41(BP5). First three binding pockets were considered for docking analysis. Binding pocket-1 is both the largest and closest to the active site. IFD docking scores of the Schiff base at three binging pockets were listed in Table 1. The binding mode of the Schiff bases into the binding pocket-1 was given in Fig. 9.

At the binding pocket-1, H_2L^1 made hydrogen bonding with Try106 via imine nitrogen (2.24 Å), with GSH via OH group (1,83), and pi-cation interaction (6.20) with Lys67. However, L^4 made hydrogen bonding (2.73 Å) with Glu442, pi-cation interaction (3.17) with Lys67 and hydrogen bonding (2.24 Å) with water molecule. H_2L^1 interacts noncovalently with Glu442, Asp441 (charged negative), with Gln445, Thr339, Asn71, (polar), with Cys63, Val64, Val68, Try106, Pro340, Val370, Phe372 (hydrophopic). L^4 also interacts with Lys67(charged positive), with Pro368, Leu444 (hydrophopic).

According to IFD docking scores, the Schiff bases bind to binding pocket-1 more than the active site. At the active site, H_2L^1 has hydrogen bonding with Gln445 (2.01 Å), however solvent water forms a bridge between Try 114 (1.68 Å) and L^4 (2.12 Å) via hydrogen bonding. NH group of L^4 also has another hydrogen bond with water. H_2L^1 interacts non-covalently with Lys66, Lys67(charged positive), with Ser30, Thr339 (polar), with Leu33, Cys58, Val59, Try 106, Try114, Pro340, Ile343 (hydrophobic). L^4 also interacts with Arg347(charged positive), and with Ala34, Val370, Phe372 (hydrophopic). Conformational changes were observed in some residues (slightly in Lys66, Ile113, Thr339 and especially in Try106, Try114) in the interactions of inhibitor (H_2L^1) and activator (L^4) at the active site (Fig. 10A and B). The difference in the GR effect of the ligands can be explained by this conformational change [35]. Changes of conformation of Lys66, Lys67, Glu442 and Gln445 before (free human GR) and after (in the presence of L^4) have also been given in Fig. 10C. For example, torsion angle CCCC at Gln445 changed from 67.6° in free human GR to −163.2° in the presence of L^4.

Table 1
Docking scores of the compounds in the active site of human GR (PDB:1GRA).

	Glide/IFD Docking Score(kcal/mol)			
Compounds	Binding pocket-1	Binding pocket-2	Binding pocket-3	Active site
H_2L^1	−10.699	−7.638	−6.994	−7.529
H_2L^2	−9.061	−6.908	−5.566	−7.054
L^3	−7.431	−6.129	−4.286	−6.566
L^4	−9.110	−8.371	−6.222	−7.911
P	−4.511	−6.372	−7.742	−5.101
QC	−7.118	−6.305	−8.433	−4.147

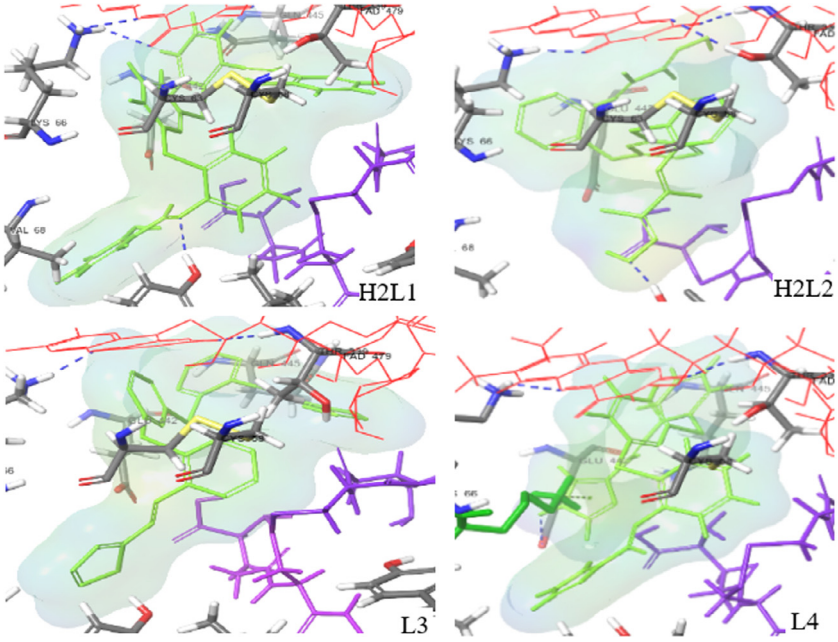

Fig. 9. Molecular docking of the Schiff bases at binding pocket-1 of GR (PDB:1GRA), FAD (red), Schiff base (green), GSSH (violet).

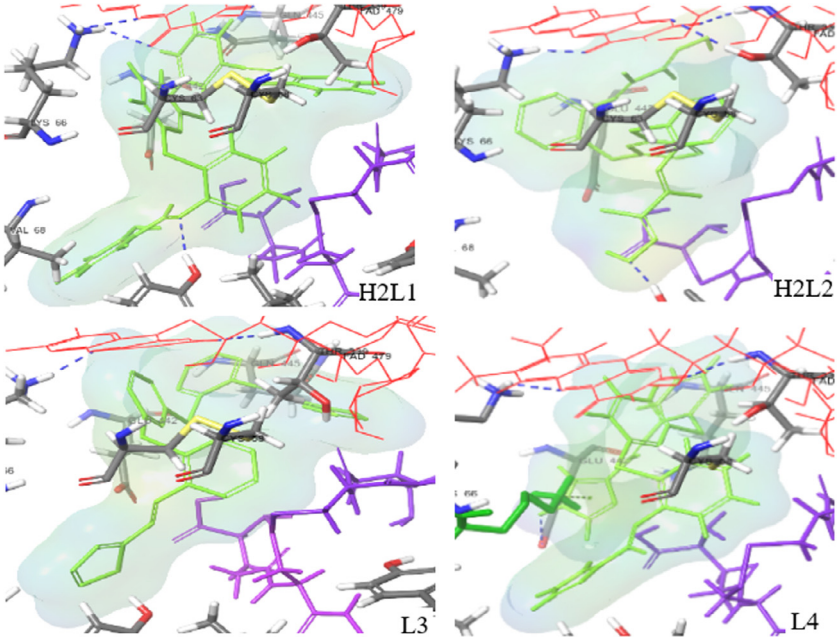

Fig. 10. Conformational change of some amino acids at (A) the active site, (B) at the binding site for H_2L^1 (yellow) and L^4, green) (C) Conformational change at binding site of some amino acids before and after the presence of L^4 (green) in human GR (blue).

Briefly, molecular docking analysis demonstrated that Schiff bases bind to binding pocket-1 rather than the active site. Moreover, conformational changes in the GR residue for H_2L^1 (inhibitor) and activator (L^4) were greater in binding pocket-1 than in the active site (Fig. 10). There are relatively few examples of small-molecular activators of enzyme activity. For example, small molecule Alda-1, acts as a structural chaperone, activates the aldehyde dehydrogenase2 by binding close to the substrate site [36]. L^4–GR complex has a distinct conformation among other Schiff bases. Also, orientation of the natural substrate at the binding pocket-1 has different conformation and different hydrophobic and polar contacts for inhibitor and activator. This conformational change observed in the activator and inhibitor can be assumed to provide a structural justification for the difference in their activity. If we compare the conformation of amino acid residue of GR-H_2L^1 (best inhibitor) and L^4 –GR (activator) complexes, Arg37, Lys66, Leu110, Ile113, Try114 show the different orientation at the active site, however, Lys66, Lys67, Leu110, Try114, Glu442, Gln445 exhibit different positions at binding pocket-1.

2.4. ADMET studies

Theoretical calculations of the ADME (absorption, distribution, metabolism and excretion) properties of the compounds were done using QikProp module. Physically significant descriptors and pharmaceutically relevant properties of the compounds obtained with QikProp are given in Table 2. As can be seen, violation of the number five rule is acceptable, that is, compounds can be predicted to

Table 2
Some descriptors and predicted properties of the compounds.

	Standart	H^2L^1	H^2L^2	L^3	L^4	P
Dipole (D)	1.0 / 12.5	10.0	2.12	3.95	4.17	7.08
IP (eV)	7.9 / 10.5	8.646	8.656	8.377	8.414	8.489
EA(eV)	−0.9 / −1.7	1.064	0.542	1.008	0.581	0.695
FOSA	0.0 – 750.0	19.191	247.038	26.862	29.591	–
FISA	7.0 – 330.0	69.158	150.490	15.546	129.854	117.845
WPSA	0.0 – 175.0	60.158	48.955	134.634	67.167	64.770
volume	500– 2000	1611.956	1518.957	1541.181	1455.516	1016.890
QPpolrz	13.0 / 70.0	57.621	49.272	55.621	51.226	34.590
MW	130.0/725.0	533.662	491.625	513.707	481.592	325.446
DHB	0.0/ 6.0	2	2	0	2	3
AHB	2.0 / 20.0	4.5	8.4	3.0	7.0	3.0
QPlogPo/w	−2 / 6.0	7.947	4.742	9.094	5.364	3.868
QPlogS	−6.5 / −0.5	−8.735	−6.045	−9.894	−6.948	−4.826
QP PCaco	25 >	2188.16	370.512	7054.726	581.426	755.752
QPlogKp	−8.0 / −1.0	0.929	−1.611	1.558	−0.905	−1.676
QPlogKhsa	−1.5 / 1.5	1.529	0.440	1.865	0.708	0.340
QPlogHERG	−5 <	−8.945	−7.010	−8.821	−8.045	−6.273
QPlogBB	−3.0 / 1.2	−0.817	−1.837	0.107	−1.339	−0.787
QPPMDCK	25 >	2463.891	313.653	10,000	642.298	827.378
CNS	−2 / +2	−1	−2	1	−2	−1
RuleOfFive		2	0	2	1	0
RuleOfThree		1	1	1	1	0

obey Lipinski's rule (MW < 500, QPlogPo/*w* < 5, donorHB ≤ 5, acceptHB ≤ 10) and to have drug-like properties. In addition, compounds are more likely to be orally available because their number of violations of Jorgensen's three rules (QPlogS > −5.7, QP PCaco > 22 nm/s, total primary metabolites < 7) is acceptable. Besides, estimated IC_{50} value for HERG K^+channels obstruction, brain-blood barrier partition coefficient, MDCK cell permeability values of all compounds are within range. Skin permeability and binding to human serum albumin values of compound L^4 are within satisfactory range.

3. Conclusion

In this study, we have synthesized new Schiff bases containing the 2,6-bis(2-aminophenylthio)pyridine unit. The compounds are characterized by X-ray crystallography and spectrophotometric methods. *in vitro* glutathione reductase activity screening against yeast and human glutathione reductase show that H_2L^1, H_2L^2 and L^3 behave as glutathione reductase inhibitors in the range of 50.09–55.23 μM for yeast GR, and in the range of 56.12– 66.87 μM for human GR. On the contrary, L^4 behaves as an activator for both yeast and human GR.

Molecular docking analysis performed with XP method at the binding site of xantane in human GR (PDB: 1XAN) show that the docking scores are as follows: xantane (−7.475) >2,6-bis(2-aminophenylthio)pyridine (−4.376) > Pyocyanin (−3.991) >Chloroquine (−2.939). Thus, it can be predicted that 2,6-bis(2-aminophenylthio)pyridine may have an antimalarial effect by binding to a different binding site than the active site. Also, based on the sequence identity and similarity between human GR (PDB:1GRA) and *P. falciparum* GR (PDB:1NOF), it can be predicted that 2,6-bis(2-aminophenylthio)pyridine may be effective on *P. falciparum.*

According to IFD docking analysis results of Schiff bases, which are non-competitive inhibitors, in the different binding pockets and active site, (a) IFD-docking scores of H_2L^1, H_2L^2 and L^3 correlates with the experimental IC_{50} value. (b) Schiff bases have a higher IFD docking score in binding pocket-1 than in the active site. (c) Schiff bases can bind to binding pocket-1 in the presence of natural substrate. (d) The conformations of the GR-ligand complexes of activator L^4 and inhibitor H_2L^1 are different from each other, which can be considered as evidence to explain the difference between activities.

L^4, an excellent activator for human GR, could be envisioned as a new candidate for the treatment of ROS-mediated oxidative damage. ADMET calculations predicted that synthesized ligands obey the Lipinski Rule (rule of five) and Jorgensen Rule (rule of three), so they could have drug-like and orally available properties.

4. Material and method

4.1. Material and instrumentation

All chemicals and glutathione reductase enzymes were purchased from Sigma-Aldrich. Solvents were of reagent grade and purified by standard procedures before use. Reactions were monitored with TLC. Elemental analysis was carried out in a Hewlett Packard 85 CHN analyzer. ESI- Mass spectra were recorded on Micro mass Quattroo LC-MS/MS spectrophotometer (Manchester, United Kingdom). ^{1}H NMR and ^{13}C NMR spectra were recorded on an Agilent 400–NMR DD2 MHz spectrometer at 400 MHz and at room temperature using d_6-DMSO solution with TMS as internal standard. IR spectra were recorded on Perkin Elmer FT-IR Spectrometer (KBr disk, 4000–400 cm^{-1}). The electronic spectra of the compounds were recorded on a Perkin Elmer Lambda 25 UV–Vis Spectrometer (USA).

4.2. Synthesis of the 2,2′-(pyridine-2,6-diyldisulfanediyl)dianiline (P)

It was synthesized for the first time and patented [37]. The solutions of 2.51 g (20 mmol) 2-Aminothiophenol in 10 ml EtOH and 1.12 g (20 mmol) KOH in 20 mL H_2O were mixed in for 30 min. To this solution 1.48 g (10 mmol) of 2,6-dichloropyridine was added portion wise and refluxed for 24 h. After this period, the precipitated light-yellow solid product was filtered *in vacuo*, washed several times with water and filtered under vacuum using a glass crucible. The obtained 1.9 g yellow solid was dried over P_2O_5 in a vacuum desiccator. Purity was checked by TLC. Its structure was elucidated using various spectroscopic methods. FT-IR (KBr,cm^{-1}): 3374–3295 (νNH_2); ^{1}H NMR($CDCl_3$)/ppm δ: 4.3(-NH_2, br. s.), 6.6–7.6(Ar-H, m.) Elemental Anal (MW: 326): Calcd. (%): C, 62.7; H, 4.6; N, 12.9 Found: C, 6.3.1; H, 4.5; N, 13.2. Structure of P is given in Fig. 1.

*4.2.1. 2,6-Bis (2-{(Z)-[(2-*sulfanylphenyl)imino*]methyl}phenol)-pyridine (H_2L^1)*

Concentrated acetic acid (1 mL) and 2.2′-(pyridine-2,6-dididisulfandiyl)dianilin (1.6 g, 5 mmol) solution in 10 ml EtOH was added dropwise to the solution of salicylaldehyde (1.22 g, 10 mmol) in 15 ml over a period of 30 min respectively. The molar ratio of Salicylaldehyde to 2,2′-(pyridine-2,6-dididisulfandiyl)dianilin is 2:1. The final mixture was refluxed for 2 h. After the precipitate, yellow solid product was filtered by vacuum filtration, washed with ethanol, recrystallized from hot acetone and dried *in vacuo* over anhydrous $CaCl_2$. FT-IR (KBr,cm^{-1}): 3350 (νOH, br), 1610 (νC = N, s); ^{13}C NMR($CDCl_3$)/ppm δ: 117.6, 118.1, 118.2, 119.1, 119.2, 119.8, 127.33 127.6, 127.7, 131.1, 131.6, 132.5, 133.6, 146.4, 161.1, 176.8; ESI-MS: m/z = 536.62 $[M + 3H]^+$, 532.74 $[M-H]^+$; UV–Vis (DMSO)/nm: 269, 275, 351; Yield: 2 g (75%); M.p. 156–157 °C; Elemental Anal (MW: 533.66), Calcd. (%): C, 69.8; H, 4.3; N, 7.9 Found: C, 70.4; H, 4.1; N, 8.1 for $C_{31}H_{23}N_3O_2S_2$.

*4.2.2. 2,6-Bis (2-{[(1Z,2E)−2-(*hydroxyimino*)−1-*methylpropylidene*]amino}-benzenethiol)pyridine (H_2L^2)*

Diacethylmonoxime (0,50 g, 5 mmol) was solved in absolute EtOH (15 mL) with adding few drops of acetic acid. After the solution of 2,2′-(pyridine-2,6-diyldisulfanediyl)dianiline (0,650 g, 2 mmol) in absolute EtOH (15 mL) was added to this mixture. The solution was stirred 12 h at room temperature. The precipitated white solid product was filtered by vacuum filtration and washed several times with ethanol, recrystallized from hot acetone and finally dried in vacuum desiccator over anhydrous $CaCl_2$. The purity was checked by TLC. FT-IR (KBr,cm^{-1}): 3200 (νOH, br), 1615 (νC = N, s); ^{13}C NMR(DMSO–d_6)/ppm δ: 39.3, 40.5, 117.7, 119.9, 120.8, 131.5, 135.3, 145.9, 149.3, 160.6, 161.7, 169.5, 181.5; ESI-MS: m/z = 550.70[M+HO.CN.CH_4]$^+$,497.20 $[M + 5H]^+$,470.23 $[M-OH-4H]^+$ 457.61 [M-2OH-5H]+; UV–Vis(DMSO)/nm: 265, 294, 349; Yield: 0.8 g (80%) M.p. 217–218 °C. Elemental Anal (MW: 491.63). Calcd.(%): C, 61.0; H, 5.1; N, 14.3 Found: C, 61.4; H, 5.4; N, 14.7 for $C_{25}H_{25}N_5O_2S_2$.

The solution of 2.2′-(pyridine-2,6-disulfandiyl)dianilin (1.6 g 5 mmol) in10 ml EtOH was added drop wise to the solution of 2-thiophenecarbaldehyde (1,12 g, 10 mmol) in 15 ml for 30 min. Then this mixture was added few drops of acetic acid. Salicylaldehyde: 2,2′-(pyridine-2,6-disulfandiyl)dianilin molar ratio of 2:1. The final mixture was refluxed for 4 h. The precipitated yellow solid product was filtered by vacuum filtration, washed with ethanol, recrystallized from hot acetone and finally dried *in vacuo* over anhydrous $CaCl_2$. The purity was checked by TLC. FT-IR (KBr,cm^{-1}):1614 (νC = N, s); ^{13}-CNMR($CDCl_3$)/ppm δ: 115.2, 118.2, 118.7, 122.8, 123.4, 131.6, 135.3, 136.8, 140.6, 148.6, 150.6, 154.5, 163.9, 182.1; ESI-MS: m/z = 514.59[$M + H$]$^+$, 512.46 $(M-H)^+$; UV–Vis(DMSO)/nm: 266, 307, 353;Yield: 1.3 g (50%); M.p. 159 °C; Elemental Anal (MW: 513.71). Calcd.(%): C, 63.1; H, 3.7; N, 8.2 Found: C, 62.8; H, 3.5; N, 8.4 for $C_{27}H_{19}N_3S_4$.

*4.2.3. 2,6-Bis (2-{[(1Z)−1H-*imidazole-4-ylmethylidene*]amino}-benzenethiol)pyridine (L^4)*

1H-imidazole-4-carbaldehyde (0,5 g, 5 mmol) was solved in absolute EtOH (10 mL) with adding 1 ml DMSO and few drops of acetic acid. After the 2,2′-(pyridine-2,6-diyldisulfanediyl)dianiline (0,81 g, 2,5 mmol) solution in absolute EtOH (10 mL) was added to mixture. The solution was boiled under reflux for 4 h. The precipitated yellow product was filtered by vacuum filtration and washed several times with ethanol, recrystallized from hot acetone and finally dried in vacuum desiccator over anhydrous $CaCl_2$. The purity was checked by TLC. FT-IR (KBr,cm^{-1}): 3145 (νOH, br), 1620 (νC = N, s); ^{13}C NMR(DMSO–d6)/ppm δ: 115.1, 116.3, 119.7, 120.3, 121.8, 125.4, 126.7, 127.4, 128.8, 131.5, 148.6, 149.7, 182.5; ESI-MS: m/z = 479.26 $(M-2H)^+$; UV–Vis(DMSO)/nm: 274, 306, 352;Yield: 0.8 g (65%); M.p. 184–185 °C; Elemental Anal (MW: 481.60). Calcd.(%): C, 62.4; H, 4.0; N, 20.4 Found: C, 62.1; H, 3.9; N, 20.7 for $C_{25}H_{19}N_7S_2$.

4.3. X-ray crystal structure determination

Single crystal X-ray measurementwere carried out on a STOEIPDS 2 diffractometer equipped with a graphite crystal monochromator at room temperature. The determination of unit cell parameters and data collections were performed with Mo$K\alpha$ radiation (λ = 0.71073 Å) at 296 K. Data collections: X-AREA and Cell refinement: X-RED32 programs [38]. The structure was solved by direct methods using SHELXS [39] and refined with SHELXL [40]. Crystal structure validations and geometrical calculations were performed using PLATON softwere [41]. All non-hydrogen atoms were refined anisotropically. All hydrogen atoms were generated geometrically and allowed to ride on their parent carbon and oxygen atoms. H atoms bonded to C atoms were located in a difference Fourier map and refined isotropically. Details of the data collection conditions and the parameters of refinement process are given in Table 1.

4.4. Glutathione reductase activity

Activity of glutathione reductase was determined according to the standard protocol [42]. Glutathione reductase activity was expressed as µmole NADPH oxidized per minute per mg protein, at pH 6.9 at 25 °C, using a molar extinction coefficient at 340 nm of 6.2 $mM^{-1}cm^{-1}$ for NADPH. Decrease in the absorbance at 340 nm due to oxidation of NADPH was monitored. The standard GR reaction medium contained 20.5 mM KH_2PO_4, 26.5 mM K_2HPO_4, 200 mM KCl, 1 mM EDTA, (pH 6.9), yeast GR (1.0 units/mL), NADPH (0.2 mM), GSSG (1 mM). The final volume of the assay mixture was 1.0 mL. The reaction mixture was carefully mixed and after a 3 min pre-incubation at 25 °C, the reaction was started by the addition of NADPH, and time-dependent changes in absorbance at 340 nm were monitored. GR activity was measured for 1 min in the quartz cuvette. The reaction was linear during this time period. The initial velocity of GR reaction was measured by the slope of recorded tracing. Ten measurements were performed and mean values were used for each data point. GR activity of control measured without addition of our complexes was equal to about 18 µmol NADPH per min per mg protein. The enzyme activities in the absence of the inhibitors were taken as 100%. 1 mM stock solutions of the compounds were prepared by dissolving in minimum amount of dimethyl sulfoxide (DMSO) and diluting with water.

4.5. Molecular modeling study

The crystal structure of human GR (PDB ID: 1GRA) was obtained from RCSB Protein Data Bank. Structure was prepared for docking using the Protein Preparation Wizard of Maestro (Schrödinger Release, 2021–1) [35]. Protein structures was corrected by adding hydrogen atoms and missing residues, assigning bond orders and bond length, creation of disulphide bonds, fixing of the charges and refining the loop with Prime and finally minimized by using OPLS-2005force field at pH of 7.4.

The 3-D models of the ligands were created using MacroModel embedded Schrödinger suite and prepared for docking using LigPrep to include possible ionization and tautomeric states, and optimized using OPLS_2005 force field. In this process, the ionization and tautomeric states were generated by Epik v5.3.

Binding sites of the human GR (1GRA) was analyzed using SiteMap module of Maestro. SiteScore and Dscore of the sites were calculated using the default parameter. After that, ligands were

docked to the grids prepared Grid generation module of Maestro using default parameter for top-ranked three binding pockets. Docking analysis was performed by Glide in Schrödinger suite [35] at extra-precision mode (XP) using OPLS_2005 force field. After evaluation of the determined XP docking scores, the best poses of the ligands were re-docked using induced fit docking module of Maestro.

The pharmacokinetic profile of the compounds was predicted by using Qikprop v3.6 module (Schrodinger, Inc., New York, NY, 2012). The program QikProp, calculate pharmacokinetic properties and descriptors such as hydrophobic component of the solvent accessible surface area (FOSA), hydrophilic component of the solvent accessible surface area(FISA),weakly polar component of the solvent accessible surface area (WPSA), predicted polarizability (QPpolrz), octanol/water partitioning coefficient (QPlogP), aqueous solubility (QPlogS), brain/blood partition coefficient (QPlogBB), human serum albumin binding (QPlogKhsa) QPlogKp: predicted skin permeability (logK_p), predicted Caco-2 cell permeability (QP PCaco), predicted IC_{50} value for blockage of HERG K^+ channels (QPlogHERG), predicted apparent MDCK cell permeability QP-MDCK, redicted central nervous system activity CNS and others.

Declaration of Competing Interest

There are no conflicts to declare.

CRediT authorship contribution statement

Turgay Tunc: Visualization, Investigation. **Ahmet Bugra Ortaakarsu:** Formal analysis. **Seda Muhsir Hatipoglu:** Investigation. **Uğur Kazancı:** Formal analysis. **Serdar Karabocek:** Conceptualization, Supervision. **Nevin Karabocek:** Investigation. **Necmi Dege:** Formal analysis. **Nurcan Karacan:** Writing – review & editing.

Acknowledgement

The authors are very grateful to TUBITAK Research Project for providing financial support (Project No. 115Z017).

Supplementary materials

CCDC 1507027contains supplementary crystallographic data (excluding structure factors) for the compound reported in this article. These data can be obtained free of charge via http://www.ccdc.cam.ac.uk/deposit [or from the Cambridge Crystallographic Data Center (CCDC), 12 Union Road, Cambridge CB2 1EZ, UK; fax: +44(0)1223 336,033; e-mail: deposit@ccdc.cam.ac.uk].

Supplementary material associated with this article can be found, in the online version, at doi:10.1016/j.molstruc.2021.132299.

References

[1] G.J. Burton, E. Jauniaux, Oxidative stress, Best Pract. Res. Clin. Obstet. Gynaecol. 25 (3) (2011) 287–299.
[2] A. Belenguer-Varea, F.J. Tarazona-Santabalbina, J.A. Avellana-Zaragoza, M. Martinez-Reig, C. Mas-Bargues, M. Ingles, Oxidative stress and exceptional human longevity: systematic review, Free Radic. Biol. Med. 149 (2020) 51–63.
[3] R. Choghakhori, A. Abbasnezhad, A. Hasanvand, R. Amani, Inflammatory cytokines and oxidative stress biomarkers in irritable bowel syndrome: association with digestive symptoms and quality of life, Cytokine 93 (2017) 34–43.
[4] S. Chakraborti, T. Chakraborti, D. Chattopadhyay, C. Shaha, Oxidative stress in microbial diseases, Springer 2019.
[5] D.A. Dickinson, H.J. Forman, Glutathione in defense and signaling lessons from a small thiol, Ann. N. Y. Acad. Sci. 973 (2002) 488–504.
[6] R. Bhowmick, R.R. Sarkar, Differential suitability of reactive oxygen species and the role of glutathione in regulating paradoxical behavior in gliomas: a mathematical perspective, PLoS ONE 15 (6) (2020) e0235204.
[7] H.J. Fan, Z.B. Tan, Y.T. Wu, X.R. Feng, Y.M. Bi, L.P. Xie, W.T. Zhang, Z. Ming, B. Liu, Y.C. Zhou, The role of ginsenoside Rb1, a potential natural glutathione reductase agonist, in preventing oxidative stress-induced apoptosis of H_9C_2 cells, J. Ginseng Res. 44 (2) (2020) 258–266.
[8] E. Kocaoglu, O. Talaz, H. Cavdar, M. Senturk, C.T. Supuran, D. Ekinci, Determination of the inhibitory effects of N-methylpyrrole derivatives on glutathione reductase enzyme, J. Enzyme Inhib. Med. Chem. 34 (1) (2019) 51–54.
[9] D. Gupta, D.P. Pathak, G. Kapoor, R. Bhutani, A comprehensive review on synthesis and biological activity of Schiff bases, Int. Res. J. Pharm. 10 (5) (2019) 1–8.
[10] L.K.A. Karem, F.Y. Waddai, N.H. Karam, Schiff base complexes of some drug substances (Review), J. Pharm. Sci. Res. 10 (8) (2018) 1912–1917.
[11] Y. Toubi, F. Abrigach, S. Radi, F. Souna, A. Hakkou, A. Alsayari, A. Bin Muhsinah, Y.N. Mabkhot, Synthesis, antimicrobial screening, homology modeling, and molecular docking studies of a new series of Schiff base derivatives as prospective fungal inhibitor candidates, Molecules 24 (18) (2019) 3250–3265.
[12] K.C. Gan, K.M. Sim, T.M. Lim, K.C. Teo, Synthesis, cytotoxic, antibacterial and free radical scavenging activities of New 1,2,4-triazole Schiff bases, Lett. Org. Chem. 17 (3) (2020) 191–198.
[13] C.C. Login, I. Baldea, B. Tiperciuc, D. Benedec, D.C. Vodnar, N. Decea, S. Suciu, A novel thiazolyl schiff base: antibacterial and antifungal effects and *in vitro* oxidative stress modulation on human endothelial cells, Oxid. Med. Cell Longev. 2019 (2019) 1–11.
[14] H.T. Balaydin, M. Ozil, M. Senturk, Synthesis and glutathione reductase inhibitory properties of 5-methyl-2,4-dihydro-3H-1,2,4-triazol-3-one's aryl Schiff base derivatives, Arch. Pharm. (Weinheim) (2018) 1–8.
[15] J.P. Legros, J.M. Fabre, L. Kaboub, 2,3-Bis(2-cyanoethylsulfanyl)-6,7-tetramethylenetetrathiafulvalene, Acta Cryst. E63 (8) (2007) o3572 o3572.
[16] I. Brito, A. Mundaca, A. Cárdenas, M. López-Rodríguez, D. Vargas, 5,5′-Dinitro-2,2′-dithiodipyridine, Acta Cryst. E63 (8) (2007) o3351–o3352.
[17] K.E. Holmes, L.M. Gilby, J.M. Stonehouse, P.F. Kelly, M.R.J. Elsegood, The preparation and crystal structures of derivatised sulfimidium salts, CrystEngComm 6 (8) (2004).
[18] S.R. Chena, F.J. Shena, G.L. Feng, R.X. Yuanb, Synthesis and anticancer activity of 4-azasteroidal-20-oxime derivatives, J. Chem. Res. 39 (2015) 527–530.
[19] V. Vijayendar, S.S. Kaki, R.C.R. Jala, Y. Poornachandra, C.G. Kumar, R.B.N. Prasad, Synthesis, characterization and biological evaluation of undecenoic acid based oxime esters, Indian Am. J. Pharm. 5 (11) (2015) 3541–3551.
[20] D. Ekinci, M. Senturk, Assesment of metal inhibition of antioxidant enzyme glutathione reductase from rainbow trout liver, J. Enzyme Inhib. Med. Chem. 28 (1) (2013) 11–15.
[21] M. Senturk, O. Talaz, D. Ekinci, H. Cavdar, O.I. Kufrevioglu, *In vitro* inhibition of human erythrocyte glutathione reductase by some new organic nitrates, Bioorg. Med. Chem. Lett. 19 (13) (2009) 3661–3663.
[22] R. Cakmak, S. Durdagi, D. Ekinci, M. Senturk, G. Topal, Design, synthesis and biological evaluation of novel nitroaromatic compounds as potent glutathione reductase inhibitors, Bioorg. Med. Chem. Lett. 21 (18) (2011) 5398–5402.
[23] P. Guller, M. Karaman, U. Guller, M. Aksoy, O.I. Kufrevioglu, A study on the effects of inhibition mechanism of curcumin, quercetin, and resveratrol on human glutathione reductase through *in vitro* and *in silico* approaches, J. Biomol. Struct. Dyn. 39 (5) (2021) 1744–1753.
[24] T. Muller, L. Johann, B. Jannack, M. Bruckner, D.A. Lanfranchi, H. Bauer, C. Sanchez, V. Yardley, C. Deregnaucourt, J. Schrevel, M. Lanzer, R.H. Schirmer, E. Davioud-Charvet, Glutathione reductase-catalyzed cascade of redox reactions to bioactivate potent antimalarial 1,4-naphthoquinones-a new strategy to combat malarial parasites, J. Am. Chem. Soc. 133 (30) (2011) 11557–11571.
[25] D.M. Stevens, R.M. Crist, S.T. Stern, Nanomedicine reformulation of chloroquine and hydroxychloroquine, Molecules 26 (175) (2020) 1–26.
[26] S. Aggarwal, D. Paliwal, D. Kaushik, G.K. Gupta, A. Kumar, Pyrazole Schiff base hybrids as anti-malarial agents: synthesis, *in vitro* screening and computational study, Comb. Chem. High Throughput Screen. 21 (3) (2018) 194–203.
[27] H. Bauer, K. Fritz-Wolf, A. Winzer, S. Kühner, S. Little, V. Yardley, H. Vezin, B. Palfey, R.H. Schirmer, E. Davioud-Charvet, A fluoro analogue of the menadione derivative 6-[2′-(3′-*methyl*) -1′,4′-*naphthoquinolyl*]hexanoic acid is a suicide substrate of glutathione reductase. Crystal structure of the alkylated human enzyme, J. Am. Chem. Soc. 128 (33) (2006) 10784–10794.
[28] D.M. Kasozi, S. Gromer, H. Adler, K. Zocher, S. Rahlfs, S. Wittlin, K. Fritz-Wolf, R.H. Schirmer, K. Becker, The bacterial redox signaller pyocyanin as an antiplasmodial agent: comparisons with its thioanalog methylene blue, Redox Rep. 16 (4) (2011) 154–165.
[29] A. Schonleben-Janas, P. Kirsch, P.R.E. Mittl, R.H. Schirmer, R.L. Krauth-Siegel, Inhibition of human glutathione reductase by 10-arylisoalloxazines crystallographic, kinetic, and electrochemical studies, J. Med. Chem. 39 (1996) 1549–1554.
[30] S.N. Savvides, P.A. Karplus, Kinetics and crystallographic analysis of human glutathione reductase in complex with a xanthene inhibitor, J. Biol. Chem. 271 (1996) 8101–8107.
[31] H. Gallwitz, S. Bonse, A. Martinez-Cruz, I. Schlichting, K. Schumacher, R.L. Krauth-Siegel, Ajoene is an inhibitor and subversive substrate of human glutathione reductase and trypanosoma cruzi trypanothione reductase: crystallographic, kinetic, and spectroscopic studies, J. Med. Chem. 42 (1999) 364–372.
[32] S.C. Yu, I.C. Kim, K.J. Ri, J. Ri, H. Kuhn, New insight into the role of glutathione reductase in glutathione peroxidase-like activity determination by coupled reductase assay: molecular docking study, J. Inorg. Biochem. 215 (2021) 111276.
[33] F. Iribarne, M. Paulino, S. Aguilera, O. Tapia, Assaying phenothiazine derivatives as trypanothione reductase and glutathione reductase inhibitors by theoretical docking and molecular dynamics studies, J. Mol. Graph. Model. 28 (4) (2009) 371–381.

[34] Schrödinger Release (2021-1): SiteMap, LigPrep v5.3; Glide v8.8; Maestro v4.3, Qikprop v3.6 LLC, New York, NY, 2021.
[35] R.L. Krauth-Siegel, L.David Arscott, A. Schönleben-Janas, R.H. Schirmer, C.H. Williams, Role of active site tyrosine residues in catalysis by human glutathione reductase, Biochemistry 37 (1998) 13968–13977.
[36] S. Perez-Miller, H. Younus, R. Vanam, C.H. Chen, D. Mochly-Rosen, T.D. Hurley, Alda-1 is an agonist and chemical chaperone for the common human aldehyde dehydrogenase 2 variant, Nat. Struct. Mol. Biol. 17 (2) (2010) 159–164.
[37] S. Karabocek, N. Karacan, U. Kazanci, N. Karabocek, Process for preparation of 2, 6- bis(2-aminophenylthio) pyridine as ligands, in: T.P. Appl. (Ed.) Turkiye, 2015, p. 10.
[38] Stoe & Cie X-AREA (Version 1.18) and X-RED 32 (Version 1.04), Stoe Cie, Darmstadt, Ger, 2002.
[39] G.M. Sheldrick, A short history of SHELX, Acta Cryst. A64 (Pt 1) (2008) 112–122.
[40] G.M. Sheldrick, Crystal structure refinement with SHELXL, Acta Cryst. C71 (Pt 1) (2015) 3–8.
[41] A.L. Spek, Structure validation in chemical crystallography, Acta Cryst. D65 (Pt 2) (2009) 148–155.
[42] L.G. Costa, E. Hodgson, D.A. Lawrence, D.J. Reed, W.F. Greenlee, Current Protocols in Toxicology, John Wiley & Sons, Inc., 2005.